Polymer Chemistry

Melt polycondensation of carboxytelechelic polyethylene for the design of degradable segmented copolyester polyolefins

Journal:	*Polymer Chemistry*
Manuscript ID	PY-ART-03-2022-000394.R1
Article Type:	Paper
Date Submitted by the Author:	04-May-2022
Complete List of Authors:	Arrington, Anastasia; Arizona State University, School of Molecular Sciences & Biodesign Center for Sustainable Macromolecular Materials and Manufacturing Brown, James; Arizona State University, School of Molecular Sciences & Biodesign Center for Sustainable Macromolecular Materials and Manufacturing Win, Max; University of Pennsylvania, Materials Science & Engineering Winey, Karen; University of Pennsylvania, Materials Science & Engineering Long, Timothy; Arizona State University, Biodesign Center for Sustainable Macromolecular Materials and Manufacturing

Melt polycondensation of carboxytelechelic polyethylene for the design of degradable segmented copolyester polyolefins

*Anastasia S. Arrington[1], James R. Brown[1], Max S. Win[2], Karen I. Winey[2] and Timothy E. Long[1]**

[1]School of Molecular Sciences & Biodesign Center for Sustainable Macromolecular Materials and Manufacturing, Arizona State University, Tempe, AZ 85281

[2]Department of Materials Science and Engineering, University of Pennsylvania, Philadelphia, PA 19104

Key words: segmented copolymer, step-growth polymerization, polyester, ring-opening metathesis

Abstract

Chain-transfer ring-opening metathesis polymerization (CT-ROMP) previously provided a route to carboxytelechelic polyethylene (PE) of controlled molecular weight; however, the incorporation of oligomeric PE into segmented copolymers remains unexplored. Herein, CT-ROMP afforded carboxytelechelic polycyclooctene segments, and subsequent reduction generated well-defined carboxytelechelic PE with M_n = 3900 g/mol. Solvent-free melt polycondensation of neopentyl glycol and adipic acid with varying wt.% telechelic PE oligomers yielded mechanically durable segmented copolyesters. The thermal and thermomechanical properties of the segmented copolyesters correlated with PE segment content, and high PE content copolymers exhibited remarkably similar morphologies and thermomechanical performance to conventional HDPE. The segmented copolyesters displayed advantageous physical properties while introducing susceptibility to chemo- and bio-catalytic depolymerization through periodic ester linkages, thus providing valuable fundamental understanding of an alternative route to HDPE.

Introduction

Ziegler-Natta catalysis enabled precise polyethylene (PE) synthesis and spurred widespread commercialization in global industries including biomedical, commodity packaging, automotive, and aerospace.[1-4] PE dominates current global plastic production, comprising 36% of all nonfiber plastic manufacturing, and PE production steadily continues to grow each year.[5] Although commodity PE in its various forms has provided tailored advantageous properties for over five decades, vigorous research continues to achieve additional tunability of molecular structure and morphology for emerging applications.[6] Recent advancements in olefin metathesis approaches, i.e., ring-opening metathesis (ROMP) and acyclic diene metathesis (ADMET), enabled the development of highly controlled polyolefin structures, permitting predictability of molecular weight, end group functionality, pendant groups, and branched topologies.[7-10] In addition, functional group periodicity within PE structure ignited exciting new directions, thus enabling development of advanced functionalized polyolefins with ionic character and excellent transport properties.[11-12] Systematic introduction of ionic sites in a periodic manner within these systems afforded unique morphology,[13-14] such as precise copolymer membranes presenting tunable ionic channels, which were suitable for fuel cell applications.[11, 15] Despite the recent advancements in PE fundamental research, improving the sustainability of commodity PE remains a global challenge; persistent issues remain due to slow degradation rates and difficult recycling due to a multitude of PE compositions.[16] Since the inception of polyolefins, 6300 Mt of plastic waste resulted , and recycling rates linger near 10%,[5] necessitating creative and innovative approaches to plastic manufacturing and sustainability. Thus, the introduction of reactive functionality within ROMP derived PE delivers new avenues for degradability of PE upon the incorporation of electrophilic linkages.

Although oxidative-based C-H activation affords PE bearing functional sites, the often uncontrolled, random addition of these functional groups limited the morphological control, thus impacting crystallizability. In contrast, development of chain-transfer (CT) ROMP protocols in previous investigations described the potential to simultaneously dictate polymer molecular weight and end group functionality on polycyclooctene (PCO).[17] Further exploration yielded carboxytelechelic PE with difunctional carboxylic acid-containing CTAs during PCO synthesis and subsequent hydrogenation.[18] Initial application of oligomeric telechelic PE structures enabled the construction of crosslinked elastomers, which displayed control of network structure as a function of targeted molecular weight.[19-20] A similar ROMP-based approach demonstrated amine end groups with application of protecting group chemistry.[21] Furthermore, telechelic diol functionalities from CT-ROMP introduced ROP initiating sites for ABA triblock construction.[22] CT-ROMP methodologies offer a well-controlled methodology for fabrication of telechelic PE.

Recyclability and degradability represent key design elements of polymer structure for converging sustainability with polymer manufacturing. Polyesters in particular provide a robust platform for recyclable materials, exemplified by the high recycling rate of polyethylene terephthalate (PET) and efficient Volcat depolymerization processes.[23-24] Our research group previously illustrated the wide range of properties and applications achievable with polyester backbones through precise monomer selection and topology control. Several examples include amorphous pressure-sensitive adhesives,[25] liquid crystalline polyesters,[26-29] ionomers,[30-32] heavily branched polyesters,[33-37] 3D printable tissue scaffolds,[38] and various segmented copolyesters.[39-41] The inherent hydrolyzability of ester linkages facilitates a multitude of pathways to depolymerization, including several chemical and enzymatic approaches.[42-43] The vast diversity of chemical structures and resulting physical properties of polyesters combined with a circular

approach to depolymerization and upcycling continues to spur interest in expanding the use of polyesters beyond their current applications. Segmented copolymers with polyester segments offer much opportunity in this regard, due to the ability to combine polyesters with other polymer backbones for specific application targeting.

Precise control of polymer architecture driven by selective chemistry allows construction of segmented copolymers, which offer many advantages over their homopolymer counterparts. Segmented copolymers are typically synthesized via condensation polymerization and consist of hard and soft segments which impart enhanced mechanical performance due to formation of microphase separated morphology.[44] Our research group previously demonstrated expertise in this area through studies of several segmented systems, including polyesters and polyurethanes exhibiting linear or branched topology.[37, 39-41, 45] Controlling segment composition and length provides tunability of glass transition temperature as well as crystallinity, enabling targeting of polymer properties for specific applications. For example, the segmented copolymer poly(ether-*block*-amide) exhibits thermoplastic elastomers properties, which enable applications in gas separation, biomedical devices, packaging, automotive parts, as well as construction materials.[46] Combining the modularity of segmented systems with excellent physical properties of polyolefins creates opportunities for novel functional materials.

Although the potential for creating new PE-based copolymers with main chain functionality from CT-ROMP is well established, segmented copolymers obtained with this synthetic method have not been thoroughly explored. A multi-block copolymer series composed of telechelic PE and PET blocks was explored as compatibilizers for PET and PE waste; however, the intrinsic properties of these copolymers were not thoroughly studied.[47] One approach to generating aliphatic long-chain polyesters involved traditional ROMP copolymerization of the lactone monomer

ambrettolide with cyclooctene.[48] Control of the methylene-to-ester ratio modulated ester integration, steering melting temperature and lamellar thickness of PE segments with higher ester content decreasing both quantities. An alternate approach to ester linkage incorporation within PE involved olefin cross metathesis of an unsaturated polyester with 1,4-polybutadiene and subsequent hydrogenation.[49] Due to the random distribution of ester linkages inherent to both methods, the length of PE segments varied widely. Thus, variability in PE segment length influenced crystallizability due to diminishing periodicity within the polymer structure. Furthermore, previous investigations of segmented polyester and polyamide systems containing fixed hydrocarbon lengths featured challenging multi-step monomer syntheses and were limited to relatively short aliphatic chains, up to 32 methylene units.[50-51]

Herein, combining protocols yielding carboxytelechelic PE oligomers with neopentyl glycol and adipic acid in solvent-free melt polycondensation provided a highly modular platform for segmented copolyesters. Contrary to previous methods, which display limited control over placement of ester linkages in PE, a step-growth methodology provides control of PE segment length. A systematic study of the influence of varying PE content allowed fundamental studies to reveal effects on thermal, mechanical, and morphological properties as a function of PE loading during melt polycondensation. In addition, incorporation of hydrolyzable ester sites within PE copolymer main chain provided a route to degradation, offering a pathway to sustainability in addition to unique copolymer composition.[52]

Experimental

Materials: Cyclooctene (95%) was purchased from Acros Organics and distilled over CaH_2 prior to use. Grubbs 2nd generation catalyst (G2) was purchased from Sigma Aldrich and stored in a glovebox to avoid degradation. Adipic acid (>99%) and maleic acid (>99%) were purchased from

TCI and recrystallized in DI water prior to use. A mixture of xylene isomers (ACS reagent grade, 98.5%) was purchased from VWR and used without further purification. Titanium tetraisopropoxide (Ti(*i*PrO)$_4$) (99.999%) was purchased from Sigma Aldrich and used as received. *p*-toluenesulfonyl hydrazide (98%) was purchased from BeanTown Chemical and used as received. The reagents 2,2-dimethylpropane-1,3-diamine (neopentyl glycol) (99%) and triethylamine (NEt_3) (99.7%) were purchased from Acros Organics and used as received. Tetrahydrofuran (THF) (99.5% stabilized with BHT) was purchased from Acros Organics and filtered through a column of alumina with N_2 prior to usage. The commercial HDPE control sample exhibited a complex viscosity of 1200 Pa·s in a time sweep melt rheology experiment conducted at 170 °C using 0.1% strain at 1 Hz. DSC measurements of the same HDPE sample revealed T_m = 130 °C and T_c = 118 °C.

Carboxytelechelic PCO synthesis: A 500-mL round-bottomed flask with a Schlenk adaptor was loaded with maleic acid (10.5 g, 90.7 mmol) under N_2 purge, followed by THF (290 mL) and distilled cyclooctene (118 mL, 907 mmol). The mixture was bubbled with N_2 gas using a 30-mm needle for 15 min. During the N_2 purge, the G2 catalyst (38 mg, 0.045 mmol) was weighed in a glovebox into a 2-mL vial. The catalyst was dissolved in 0.7 mL THF at the end of the purge for the reaction mixture. Once N_2 flow was established through the Schlenk adaptor in the round-bottomed flask containing the reaction mixture, the catalyst solution was added quickly using a dry syringe. The reaction was stirred on the lowest setting for 18 h, precipitated dropwise into 3 L MeOH, and allowed to stir in the solvent for 4 h. The white precipitate was filtered and dried in a vacuum oven at 60 °C with 40 mmHg for 18 h. ^{1}H NMR (500 MHz, $CDCl_3$) δ 7.08 (dt, J = 14.9, 6.9 Hz, 1H), 5.83 (dd, J = 15.6, 1.6 Hz, 1H), 5.57 – 5.19 (m, 33H), 2.30 – 2.18 (m, 2H), 2.12 – 1.81 (m, 66H), 1.47 (p, J = 7.2 Hz, 3H), 1.42 – 1.11 (m, 133H). Yield = 96%

Reduction of PCO to PE: A 2-L 3-neck round-bottomed flask was loaded with PCO (45 g, 12.1 mmol), xylenes (1 L) and triethylamine (55 mL, 394 mmol). Once the mixture was fully dissolved, *p*-toluenesulfonyl hydrazide (110 g, 590 mmol) was added to the flask in 30 g increments every 30 min after the reflux began to avoid violent boiling from excessive hydrazide decomposition.[53] Following the initial loading of hydrazide (30 g, 161 mmol), the round-bottomed flask was fitted with a reflux condenser, a hose adaptor for N_2 gas, and a rubber septum. The mixture was heated to 140 °C and carefully monitored to avoid exceeding the selected temperature. After the final addition of hydrazide, an additional 100 mL of xylenes was loaded to the flask and the reaction was stirred for an additional 4 h at reflux. The mixture was cooled in an ice bath until solids formed, poured into 3 L of cold ethanol and allowed to stir 18 h. The white solid was filtered and rinsed with 200 mL of additional ethanol, then dried at reduced pressure at 90 °C for 18 h under 40 mmHg. The solid was characterized with ^{1}H NMR spectroscopy in TCE-d_2 at 100 °C. ^{1}H NMR (400 MHz, TCE-d_2) δ 2.39 (t, 2H), 1.34 (m, 259H). Yield = 93%

Synthesis of poly(neopentyl adipate) amorphous polyester: This procedure was adapted from previous works.[54] A 100-mL round-bottomed flask was charged with neopentyl glycol (5.8370 g, 1.2 mol eq), adipic acid (8.14 g, 1.0 mol eq), and Ti(*i*PrO)$_4$ catalyst (40 μg, 1.40 x 10^{-4} mmol). A slight excess of neopentyl glycol was charged relative to total carboxylic acid in the above reaction, 1.00 eq total acid to 1.20 eq neopentyl glycol, to compensate for the lower boiling point of the monomer. The reaction was purged with N_2 and degassed under 2 mmHg vacuum three times to ensure extensive removal of oxygen prior to heating. The round-bottomed flask was then lowered into a metal bath at 170 °C and allowed to proceed under N_2 purge and stirring for 2 h. The reaction temperature was then raised to 220 °C for 2 h, followed by application of 2 mmHg vacuum for an

additional 2 h. The resulting viscous polymer was removed from the round-bottomed flask and used without further purification.

Representative polycondensation procedure for segmented copolymers: All copolymers were synthesized using a melt esterification procedure. The charged wt.% telechelic PE included 10%, 48%, 75%, and 95% and subsequently referred to as the corresponding wt.% throughout the manuscript. For example, in preparation of poly(ethylene$_{75}$-co-neopentyladipate$_{25}$) where the subscript corresponds to the weight percent of each segment charged, carboxytelechelic PE (11 g, 3.05 mmol), neopentyl glycol (1.59 g, 15.3 mmol), adipic acid (1.78 g, 12.2 mmol) and Ti(*i*PrO)$_4$ catalyst (40 μg, 1.40 x 10^{-4} mmol) were added to a dry 100-mL round-bottomed flask equipped with a N_2 inlet, mechanical stirrer, and distillation apparatus. A slight excess of neopentyl glycol was charged relative to total carboxylic acid in the above reaction, 1.00 eq total acid to 1.20 eq neopentyl glycol, to compensate for the lower boiling point of the monomer.[54] The reaction was purged with N_2 and degassed under 2 mmHg vacuum three times to ensure extensive removal of oxygen prior to heating. The round-bottomed flask was then lowered into a metal bath at 170 °C and allowed to proceed under N_2 purge and stirring for 2 h. The reaction temperature was then raised to 220 °C for an additional 2 h, followed by an increase to 235 °C for 0.5 h. Vacuum was then applied while stirring at 235 °C for 2 h. The resulting copolymer was removed from the round-bottomed flask and used without further purification.

Film preparation: Following polycondensation, the polymers were removed from the stir rod and melt pressed into films on a Carver press at 150 °C with 0.01 inch shims between sheets of Kapton® film. The polymer samples were subject to 1 ton of pressure for 5 min, then 6 tons for another 5 min prior to removal and quench cooling in an ice bath.

Characterization parameters: A Bruker 500 MHz spectrometer was utilized for NMR spectroscopy. All polymer samples were analyzed in $CDCl_3$ with 128 scans and a 5 s relaxation delay. High temperature ^1H NMR experiments were performed on a Bruker 400 MHz spectrometer with 8 scans and a 1 s relaxation delay. Number-average (M_n) and weight-average (M_w) molar mass and dispersity ($Đ = M_w/M_n$) of polymers were obtained from size exclusion chromatography (SEC) using a Waters Alliance e2695 separation module outfitted with two Shodex KD-806M columns in series 8 x 300 mm). THF was used as eluent at 1 mL/min at 35 °C with sample injection volumes of 100 uL. Polystyrene standards were used to calibrate the SEC system. Analyte samples at 2 mg/mL were filtered through a poly(tetrafluoroethylene) membrane with 0.45 mm pore before injection (100 μL). A d*n*/d*c* value of 0.110 for PCO was referenced from the literature.[17] Absolute molecular weight characterization proceeded with a Wyatt miniDAWN® TREOS® II multi-angle light scattering detector. TA Instruments Discovery Series TGA5500 was employed for thermogravimetric analysis (TGA), with a 10 °C/min heating rate and N_2 atmosphere. TA Instruments Discovery Series DSC2500 was utilized for differential scanning calorimetry (DSC), with a 10 °C/min heating and 5 °C/min cooling rate for heat/cool/heat cycles. In all DSC plots, the curves are depicted with endothermic transitions up. Dynamic mechanical analysis (DMA) was conducted on rectangular samples from melt pressed films using a TA Instruments Q800 Dynamic Mechanical Analyzer in tension mode, with 0.1% strain and 1 Hz, heated from -130 °C to 200 °C at a heating rate of 3 °C/min under air. A DHR-3 rheometer was utilized for melt rheology of polymer samples. The sample conditioning was performed at 170 °C and the analysis proceeded using 0.1% strain and 1 Hz under air. Tensile testing was performed using an Instron 3343 with polymer specimens prepared according to ASTM-D638 method from melt pressed films of uniform thickness. Polymer samples were uniaxially strained at a crosshead speed of 10 mm/min

with 5 samples per composition for statistical analysis. X-ray scattering experiments were performed at room temperature on free-standing films using the Dual-source and Environmental X-ray scattering (DEXS) facility at the University of Pennsylvania. This facility is equipped with a PILATUS 1 M detector and PILATUS 100 K detector for small angle scattering (SAXS) and wide angle scattering (WAXS), respectively. The GenixX3D X-ray source (8 keV, Cu K□, □ = 1.54 Å) was used with a sample-to-detector distances of 122 cm and 15 cm to obtain q-ranges of 0.01-0.2 Å-1 and 1.1-3.2 Å-1, respectively.

Results and Discussion

Synthesis of carboxytelechelic PE prepolymers

ROMP initially produced PCO (**Scheme 1**) as an unsaturated precursor to the carboxytelechelic PE for subsequent melt reactions. CT-ROMP provides a facile pathway to fully linear carboxytelechelic PE, enabling reliable synthesis of PE segments with control over endgroup identity, functionality, and molecular weight.[18] Common endgroup functionalities with this approach include diacids and diols, in which are derived from the chain transfer agent (CTA). Maleic acid served as the CTA, providing telechelic carboxylic acid endgroups. Furthermore, the molecular weight selection proceeded through stoichiometric alteration of relative equivalents of monomer to CTA, i.e., the higher ratios providing lower endgroup concentrations and corresponding lower M_n. PCO M_n was clearly characterized by endgroup analysis from ^{1}H NMR (**Figure S1**) due to endgroup aggregation in SEC, which skewed the molecular weight upward (**Figure S2**).[18] For this study, a single M_n was selected (3,700 g/mol) for segmented copolyester synthesis, and a consistent PCO precursor was maintained to ensure reproducibility across the compositional space. The subsequent reduction of unsaturated PCO proceeded efficiently in the presence of tosyl hydrazide, which generated the expected diimide reducing agent upon thermal

decomposition.[53] Selectivity toward symmetric double bonds of this particular reducing agent provides an advantage over other common catalyst choices such as Pt-based catalysts, which also reduce carbonyls, leading to loss of targeted functionality.[53, 55] The carboxytelechelic PE oligomer was characterized with high temperature ^{1}H NMR spectroscopy (**Figure S3**), which confirmed quantitative hydrogenation and validated number-average molecular weight for melt polymerization stoichiometry to ensure high molecular weight segmented copolyesters.

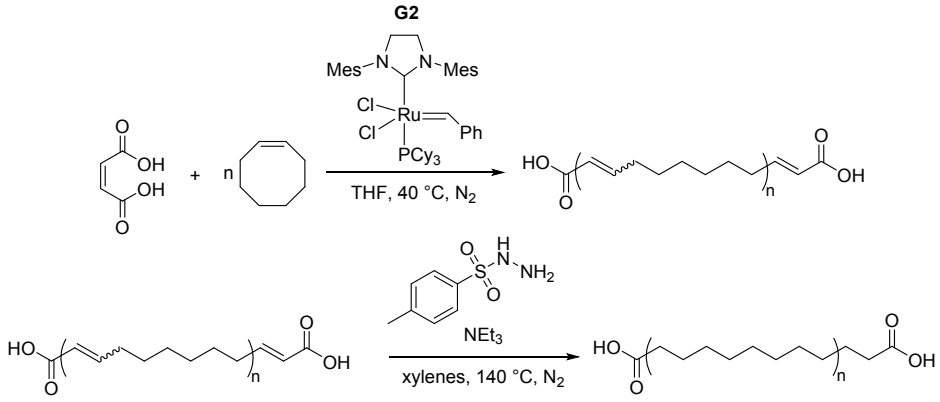

Scheme 1. Top) CT-ROMP with maleic acid CTA, providing telechelic carboxylic acid functionality. Bottom) Reduction of double bonds via diimide generation, yielding carboxytelechelic PE segments. Synthesis adapted from reference.[18]

Synthesis of amorphous polyester control and segmented copolymers

The copolymerization of long-chain aliphatic carboxytelechelic segments with various diacids and diols proceeded according to a step-growth polymerization, and monomers where selected to produce an amorphous polyester segment. An amorphous, aliphatic polyester segment offered ease of melt processability in comparison to semi-crystalline counterparts. In addition, the selected polyester segment facilitated analysis of the influence of PE composition on crystallization behavior within segmented copolymers. Due to PE serving as the only crystallizable component, the emergence of co-crystallization and other complex morphological phenomena was avoided, The synthetic investigation initially involved the polymerization of an amorphous polyester

homopolymer, i.e., poly(neopentyl adipate) (PNA) in accordance with our previous work (**Scheme 2)** to probe the thermal properties of the homopolymer.[54]

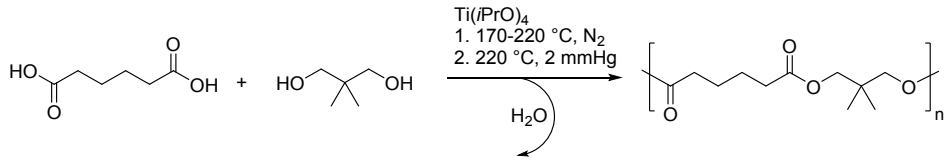

Scheme 2. Polycondensation of the amorphous polyester PNA, synthesized using 1:1.2 stoichiometry of diacid:diol. Synthesis adapted from our earlier efforts.[54]

Segmented copolymers with varying wt.% PE loading were prepared similarly to the amorphous polyester control using a melt condensation approach (**Scheme 3**), with marginally higher top temperatures (235 °C) due to higher viscosities reached at high conversion. The resulting solids displayed mechanical robustness upon removal from the glassware, and a slight yellow color, primarily originating from catalyst selection and residual oxygen. The application of antimony-based catalyst may improve the color in future segmented copolymer syntheses outside of this work.[56]

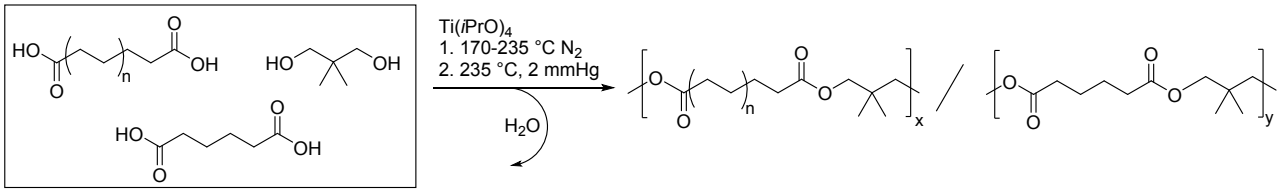

Scheme 3. Polycondensation of carboxytelechelic PE segments with adipic acid and neopentyl glycol provides segmented copolyesters.

Thermal characterization of copolymers and corresponding controls

Design of segmented copolyesters with PE segments of fixed length enabled the elucidation of thermal properties with varying PE levels. TGA profiles, as depicted in **Figure 1,** displayed a compositional dependency, revealing weight loss behavior consistent with the amorphous

polyester level as well as the carboxytelechelic PE component. The amorphous polyester control displayed a single weight loss step with $T_{d,5\%}$ at 324 °C, while the carboxytelechelic PE $T_{d,5\%}$ occurred at 435 °C. Most segmented copolyester compositions exhibited two weight loss steps apart from the 95 wt.% PE loading (**Table S1**).

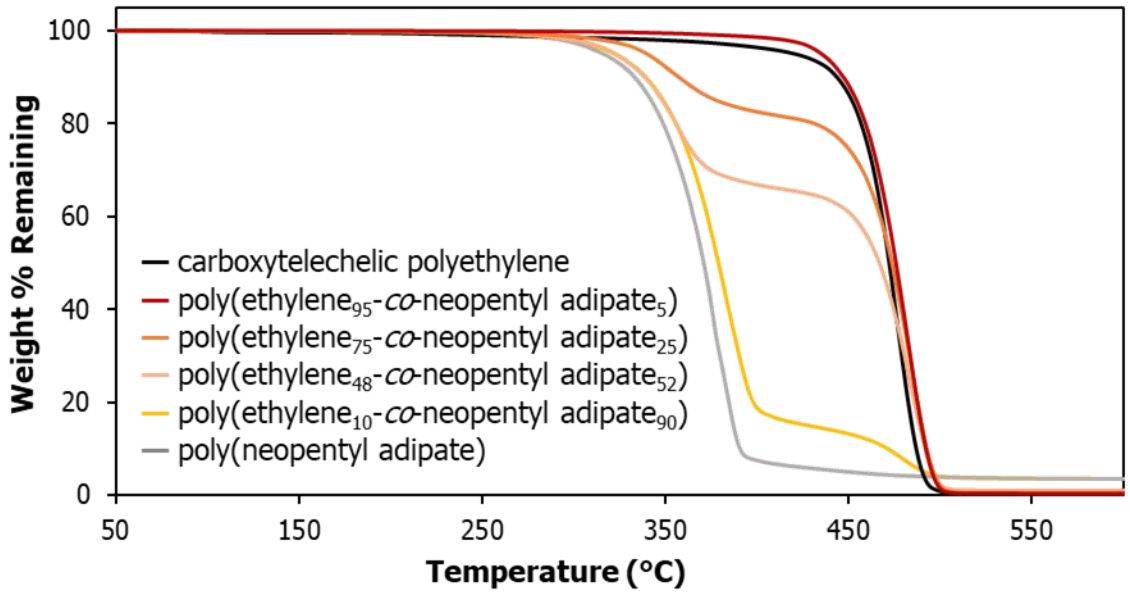

Figure 1. TGA of segmented copolymers and homopolymer controls corresponding to PE wt.% loading. All samples were tested with a heating rate of 10 °C/min.

Analysis of the segmented copolyesters and homopolymer comparisons revealed compositional influence on crystallization and melting with DSC analysis. For reference, the carboxytelechelic PE prepolymer exhibited a T_m at 130 °C with a relatively high enthalpy of melting with a value of 202 J/g (**Figure S4, Table 1**), as expected for PE with high symmetry and the absence of branching. The prepolymer exhibited 70% crystallinity according to the literature value of 286.7 J/g ΔH_f for 100% orthorhombic HDPE.[57] (Note that the orthorhombic crystal structure of the copolymers is confirmed below.) In contrast, the amorphous polyester PNA only possessed a single glass transition temperature (T_g) at -45 °C (**Figure 2**), as anticipated from our previous literature.[54]

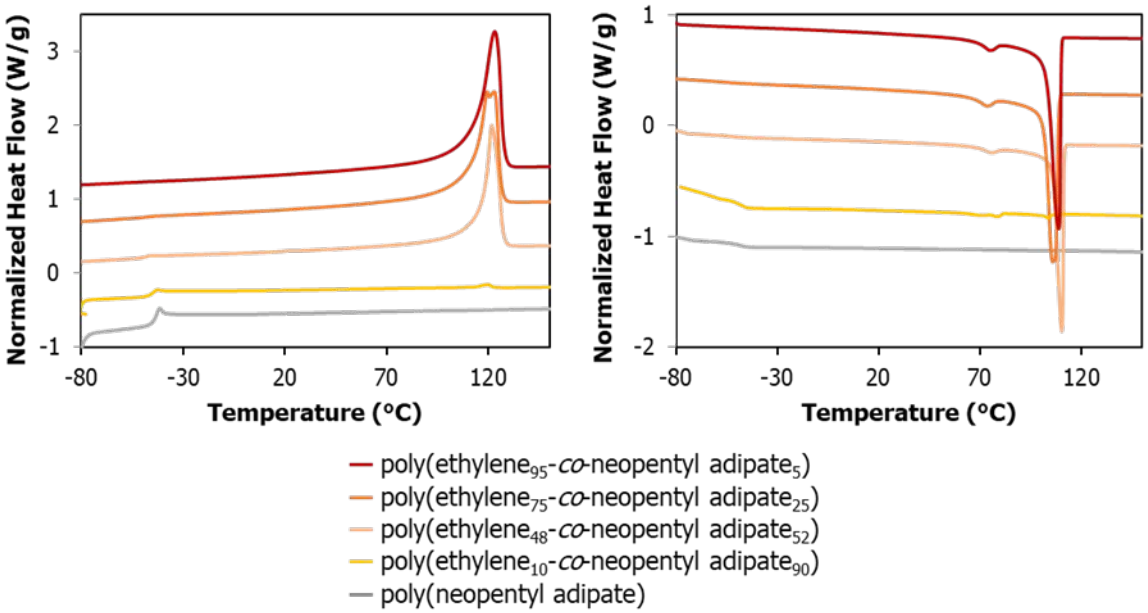

Figure 2. DSC curves displaying the (left) 2nd heating cycle and (right) cooling cycle profiles of segmented copolyesters and homopolymer controls. Endothermic transitions are depicted upwards. Samples were subject to a heat/cool/heat cycle with a heating rate of 10 °C/min and a cooling rate of 5 °C/min.

The segmented copolyester containing the lowest PE wt.% and high PNA content displayed a T_g originating from the polyester segment and a diminished T_m from the PE segment (**Table 1, Figure 2**). The intermediate composition with roughly equal wt. % polyester and PE levels displayed a less prominent T_g from the amorphous segment and more pronounced PE melting endotherm. The high PE level segmented copolyesters only exhibited a sharp PE melting endotherm with increasing enthalpy and percent crystallinity, modulated with increasing PE loading. The observed trend was consistent with increasing symmetry due to decreasing ester segment content, which effectively disrupts PE crystallization.

Table 1. Summary of thermal transitions and their enthalpies found in DSC traces of segmented copolyesters with varying wt.% PE. Percent crystallinity calculated from literature value of 286.7 J/g for 100% orthorhombic HDPE.[57]

Polymer Composition	T_m (°C)	ΔH_m (J/g)	T_c (°C)	ΔH_c (J/g)	Calc. % crystallinity
Commercial HDPE	130	183	118	177	63
HOOC-PE-COOH	130	202	117	202	70
poly(ethylene$_{10}$-*co*-neopentyl adipate$_{90}$)	120	1.5	79	1.7	-
			104	1.4	0.5
poly(ethylene$_{48}$-*co*-neopentyl adipate$_{52}$)	121	103	75	3.3	-
			110	88.5	36
poly(ethylene$_{75}$-*co*-neopentyl adipate$_{25}$)	120	137	73	5.4	-
			106	112	48
poly(ethylene$_{95}$-*co*-neopentyl adipate$_{5}$)	123	153	75	5.1	-
			109	124	53

Morphological characterization

The WAXS data for two segmented copolyesters and a HDPE sample show the presence of orthorhombic crystals with comparable unit cell dimensions and crystal sizes (**Figure 3**). The SAXS from these samples reveal long period peaks at low q, confirming their semicrystallinity. The combination of % crystallinity determined using DSC with the SAXS profiles led to the calculation of estimated crystalline thickness, which increased with decreasing heteroatom linkage content, with the commercial HDPE exhibiting the highest value (**Table S2**). The thermal history of the melt pressed films utilized in the SAXS analysis heavily influences the crystallization and resulting crystal size; the quench cooling treatment of the polymer films prior to analysis employed herein could yield distinct results from a slowly-cooled series of the same polymers. Elucidation of the effects of these differences in cooling rate on crystal size may be pursued in future works.

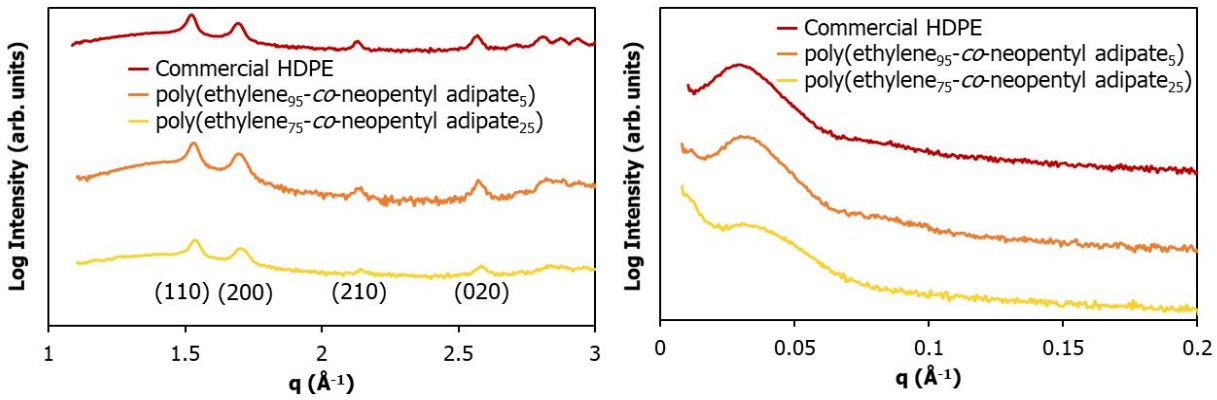

Figure 3. Scattering profiles comparing two segmented copolyesters and an HDPE control obtained via (left) WAXS and (right) SAXS confirm the orthorhombic unit cell and a semi-crystalline morphology. Data has been shifted vertically for clarity.

Thermomechanical analysis of segmented copolyesters

Tensile testing and DMA collectively revealed the relationship between PE content and mechanical performance. Tensile testing revealed a trend in both strain at break and Young's modulus among compositions with increasing PE wt.% displaying a consistently higher % strain at break and a decreasing Young's modulus (**Figure 4**). Compositions below 48 wt.% PE failed to form free-standing films due to lack of sufficient crystallinity, which serve as physical crosslinks. The carboxytelechelic PE control exhibited insufficient M_n for film formation, therefore only high levels of PE were tested. A commercial HDPE sample served as a benchmark, and the data illustrated the similarity in yield behavior of the segmented homopolymers with 75 and 95% wt.% PE, which was significantly less than the high elongations for the commercial sample by about 50-60%. Conversely, the 48 wt.% PE copolymer demonstrated significant embrittlement compared to the remaining segmented copolymer compositions with higher maximum stress and lower % strain at break. The tensile experiment exemplified the necessary delicate balance between PE wt.% and ester content, providing samples with sufficient mechanical integrity with incorporated ester linkages. This balance appeared to reside closer to high PE wt.% levels over the compositional range.

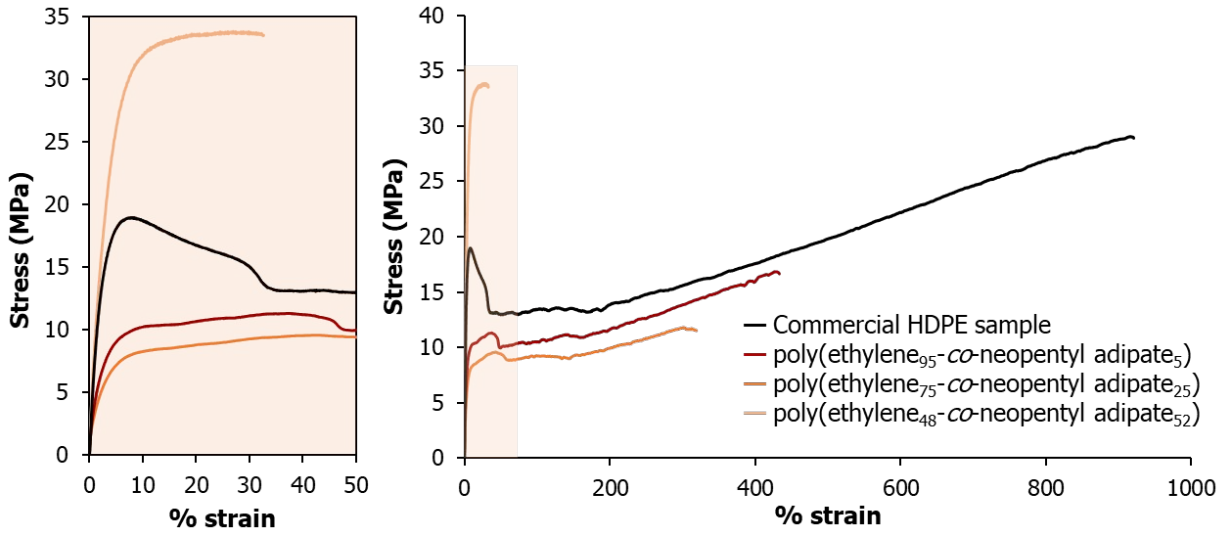

Figure 4. Tensile curves of segmented copolymers containing varying wt.% PE incorporation. One representative sample displayed for each composition, n = 5, 10 mm/min crosshead speed.

Table 2. Summary of tensile properties measured for segmented copolyesters and a HDPE commercial sample. Samples were tested using crosshead speed of 10 mm/min and all table values contain 5 samples per composition.

Sample	% strain at break	Young's Modulus (MPa)	Maximum stress (MPa)	Stress at break (MPa)
poly(ethylene$_{48}$-*co*-neopentyl adipate$_{52}$)	40 ± 15	820 ± 100	37 ± 6	34 ± 6
poly(ethylene$_{75}$-*co*-neopentyl adipate$_{25}$)	250 ± 100	300 ± 9	11 ± 1	10 ± 2
poly(ethylene$_{95}$-*co*-neopentyl adipate$_{5}$)	380 ± 40	450 ± 10	16 ± 1	16 ± 1
Commercial HDPE sample	800 ± 150	870 ± 60	28 ± 3	28 ± 3

DMA demonstrated intriguing trends in the transitions corresponding to the amorphous polyester segments and the PE segments within the segmented copolymers (**Figure 5**). A slight decrease in modulus at -110 °C suggested the ɣ-relaxation of the amorphous PE phase,[58] which

was visible in all segmented copolymers, and as expected, more pronounced in the highest PE wt.% composition. The T_g of the amorphous polyester segment emerged at -35 °C for the 75 and 48 wt.% PE, the latter demonstrating greater peak intensity in tanδ. The composition containing only 5 wt.% of amorphous polyester segment did not display a T_g, presumably due to the amorphous segments lacking sufficient length, thus only serving as linkers for the PE segments. The final broad transition occurring prior to flow and subsequent sample failure corresponds to the α-relaxation of the PE crystalline phase, and it appeared at different temperatures for all three segmented copolymer compositions with peak temperatures of 82, 53, and 69 °C for 48, 75, and 95 wt.% PE copolymers, respectively. A trend occurred in the E' at room temperature with higher wt.% PE exhibiting higher E' values. While the 48 and 75 wt.% PE compositions were relatively close at 298 and 348 MPa, respectively, the 95 wt.% PE copolymer displayed a storage modulus of 662 MPa. Additionally, the onset temperature for viscous flow varied by composition; the highest melting temperature of 122 °C from the 95 wt.% PE copolyester, the others displaying melting temperatures as low as 110 °C. The difference in flow onset temperature and room-temperature E' may suggest differences in molecular weight for the various segmented copolyesters. The thermomechanical profiles corroborated the findings from tensile experiments, indicating that higher wt.% PE segmented copolymers displayed improved performance compared to lower PE levels.

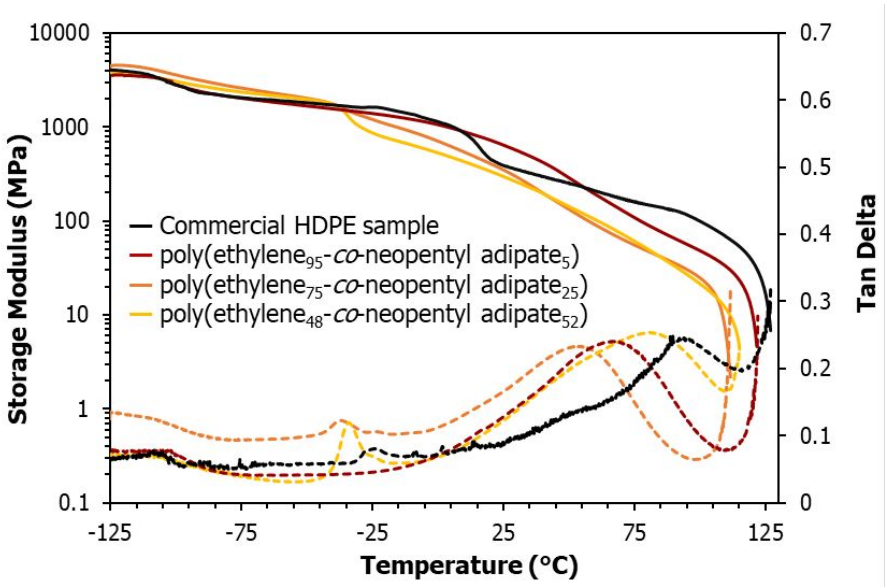

Figure 5. DMA of segmented copolymers containing 48, 75, and 95 wt.% PE loading. The solid lines represent the storage modulus, while the dotted lines signify tanδ. All samples tested at a heating rate of 3 °C/min.

All segmented copolyesters were further analyzed with melt rheology to probe differences in their melt viscosity and melt stability to garner insight into potential melt processability. The complex viscosity at 170 °C consistently increased with increasing wt.% PE (**Figure S5**). However, the potential for variability in molecular weight presented challenges in differentiating the role of chemical structure across this observed trend. Notably, the HDPE control sample exhibited the same melt viscosity as the 48 wt.% PE containing segmented copolymer. The same rheology experiment enabled analysis of the G' and G" as a function of time, displaying a gradual increase in the G' , eventually crossing over the G" after 45 min to 1 h depending on composition. Addition of antioxidants and stabilizers that are commonly necessary in an industrial setting may alleviate the lack of thermal stability under air in addition to processing under an inert atmosphere.[59-60]

Preliminary experiments describing chemical depolymerization of segmented copolyesters demonstrate the ability to recover the PE prepolymer following hydrolysis of the copolymer (**Figure S6**). Similar chemical depolymerization pathways were previously described for polyolefins with shorter aliphatic chains between ester or carbonate linkages, exhibiting good mechanical performance of the recycled material.[61] We aim to demonstrate the potential to reform segmented copolymers from recovered telechelic PE; however, the depolymerization described herein requires larger scales to generate sufficient polymer for further melt reactions. Future work in this area entails further understanding of depolymerization kinetics of segmented copolymers as a function of composition, in addition to recycling potential of the resulting prepolymers.

Conclusions

The application of CT-ROMP of cyclooctene in combination with hydrogenation enabled the synthesis of carboxytelechelic PE segments, which produced segmented copolyesters upon melt polycondensation in the presence of diacid and diol monomers. Previous investigations of segmented copolyesters either contained significantly shorter aliphatic chains between ester units, thus limiting crystallizability, or lacked the precise segment length control demonstrated herein. Segmented copolyesters synthesized in this study comprised of amorphous polyester and linear PE segments and exhibited thermal properties modulated by their wt.% PE levels in addition to progressively improved mechanical performance with increasing wt.% PE content. DMA displayed transitions from both the polyester and PE segments as well as dependence of composition on E'. Rheological melt stability studies demonstrated an acceptable melt processing window prior to crosslinking, displaying suitability for future melt processing with room for improvement with antioxidant formulation and level of PE incorporation. This work establishes a platform for creating custom PE-based segmented copolyesters with degradable ester linkages and

potential to easily incorporate branched architecture through the ester monomers rather than multi-step strained cyclic monomer functionalization.[19] Control of PE crystallization and segment size provides modularity for targeting specific physical properties of the final product. Further structural tuning with other diols and diacids as well as amide linkages will provide additional insight into structure-property relationships within these novel segmented systems.

Conflicts of Interest

There are no conflicts of interest to declare.

Acknowledgements

M.S.W. and K.I.W. acknowledge the NSF DMR (1904767) and the NSF MRSEC (17-20530), NSF MRI (17-25969), and ARO DURIP grants (W911NF-17-1-0282) for the Dual Source and Environmental X-ray Scattering facility operated by the Laboratory for Research on the Structure of Matter at the University of Pennsylvania.

References

1. Knuuttila, H.; Lehtinen, A.; Nummila-Pakarinen, A., *Long Term Properties of Polyolefins* **2004**, 13-28.
2. Paxton, N. C.; Allenby, M. C.; Lewis, P. M.; Woodruff, M. A., *European Polymer Journal* **2019,** *118*, 412-428.
3. Gautam, Y.; Singh, S.; Verma, M.; Singh, A. P., **2018,** *6*, 1768-1771.
4. Sehanobish, K., Automotive Applications for Polyethylene. 2016; pp 1169-1178.
5. Geyer, R.; Jambeck, J. R.; Law, K. L., *Sci Adv* **2017,** *3* (7), e1700782-e1700782.
6. Munaro, M.; Akcelrud, L., *Polymer Degradation and Stability* **2008,** *93* (1), 43-49.
7. Choinopoulos, I., *Polymers* **2019,** *11* (2), 298.
8. Schulz, M. D.; Wagener, K. B., *Macromolecular Chemistry and Physics* **2014,** *215* (20), 1936-1945.
9. Bielawski, C. W.; Grubbs, R. H., *Progress in Polymer Science* **2007,** *32* (1), 1-29.
10. Smith, J. A.; Brzezinska, K. R.; Valenti, D. J.; Wagener, K. B., *Macromolecules* **2000,** *33* (10), 3781-3794.
11. Yan, L.; Häußler, M.; Bauer, J.; Mecking, S.; Winey, K. I., *Macromolecules* **2019,** *52* (13), 4949-4956.
12. Choi, U. H.; Middleton, L. R.; Soccio, M.; Buitrago, C. F.; Aitken, B. S.; Masser, H.; Wagener, K. B.; Winey, K. I.; Runt, J., *Macromolecules* **2015,** *48* (2), 410-420.
13. Buitrago, C. F.; Opper, K. L.; Wagener, K. B.; Winey, K. I., *ACS Macro Letters* **2012,** *1* (1), 71-74.
14. Middleton, L. R.; Trigg, E. B.; Schwartz, E.; Opper, K. L.; Baughman, T. W.; Wagener, K. B.; Winey, K. I., *Macromolecules* **2016,** *49* (21), 8209-8218.

15. Trigg, E. B.; Gaines, T. W.; Maréchal, M.; Moed, D. E.; Rannou, P.; Wagener, K. B.; Stevens, M. J.; Winey, K. I., *Nature materials* **2018,** *17* (8), 725-731.
16. Hakkarainen, M.; Albertsson, A.-C., Environmental Degradation of Polyethylene. In *Long Term Properties of Polyolefins*, Albertsson, A.-C., Ed. Springer Berlin Heidelberg: Berlin, Heidelberg, 2004; pp 177-200.
17. Grubbs, R. H.; O'Leary, D. J., *Handbook of Metathesis, Volume 2: Applications in Organic Synthesis*. John Wiley & Sons: 2015.
18. Pitet, L. M.; Hillmyer, M. A., *Macromolecules* **2011,** *44* (7), 2378-2381.
19. Martinez, H.; Hillmyer, M. A., *Macromolecules* **2014,** *47* (2), 479-485.
20. Ren, N.; Matta, M. E.; Martinez, H.; Walton, K. L.; Munro, J. C.; Schneiderman, D. K.; Hillmyer, M. A., *Industrial & Engineering Chemistry Research* **2016,** *55* (21), 6106-6112.
21. Martinez, H.; Hillmyer, M. A.; Matta, M.; Munro, J. C.; Walton, K. L., Process to produce a polyolefin reactive telechelic pre-polymer. Google Patents: 2020.
22. Arrington, K. J.; Waugh, J. B.; Radzinski, S. C.; Matson, J. B., *Macromolecules* **2017,** *50* (11), 4180-4187.
23. Allen, R. D.; James, M. I., Chemical Recycling of PET. In *Circular Economy of Polymers: Topics in Recycling Technologies*, American Chemical Society: 2021; Vol. 1391, pp 61-80.
24. Brouwer, M. T.; Alvarado Chacon, F.; Thoden van Velzen, E. U., *Packaging Technology and Science* **2020,** *33* (9), 373-383.
25. Ozturk, G. I.; Pasquale, A. J.; Long, T. E., *The Journal of Adhesion* **2010,** *86* (4), 395-408.
26. Lin, Q.; Pasatta, J.; Wang, Z.-H.; Ratta, V.; Wilkes, G. L.; Long, T. E., *Polymer International* **2002,** *51* (6), 540-546.
27. Lin, Q.; Pasatta, J.; Long, T. E., *Journal of Polymer Science Part A: Polymer Chemistry* **2003,** *41* (16), 2512-2520.
28. Heifferon, K. V.; Mondschein, R. J.; Talley, S. J.; Moore, R. B.; Turner, S. R.; Long, T. E., *Polymer* **2019,** *163*, 125-133.
29. Heifferon, K. V.; Spiering, G. A.; Talley, S. J.; Hegde, M.; Moore, R. B.; Turner, S. R.; Long, T. E., *Polymer Chemistry* **2019,** *10* (31), 4287-4296.
30. Pekkanen, A. M.; Zawaski, C.; Stevenson Jr, A. T.; Dickerman, R.; Whittington, A. R.; Williams, C. B.; Long, T. E., *ACS applied materials & interfaces* **2017,** *9* (14), 12324-12331.
31. Ju, L.; Dennis, J. M.; Heifferon, K. V.; Long, T. E.; Moore, R. B., *ACS Applied Polymer Materials* **2019,** *1* (5), 1071-1080.
32. Ju, L.; Mondschein, R. J.; Vandenbrande, J. A.; Arrington, C. B.; Long, T. E.; Moore, R. B., *Polymer* **2020,** *205*, 122891.
33. Lin, Q.; Long, T. E., *Macromolecules* **2003,** *36* (26), 9809-9816.
34. Unal, S.; Lin, Q.; Mourey, T. H.; Long, T. E., *Macromolecules* **2005,** *38* (8), 3246-3254.
35. McKee, M. G.; Unal, S.; Wilkes, G. L.; Long, T. E., *Progress in polymer science* **2005,** *30* (5), 507-539.
36. Unal, S.; Long, T. E., *Macromolecules* **2006,** *39* (8), 2788-2793.
37. Unal, S.; Ozturk, G.; Sisson, K.; Long, T. E., *Journal of Polymer Science Part A: Polymer Chemistry* **2008,** *46* (18), 6285-6295.
38. Sirrine, J. M.; Pekkanen, A. M.; Nelson, A. M.; Chartrain, N. A.; Williams, C. B.; Long, T. E., *Australian Journal of Chemistry* **2015,** *68* (9), 1409-1414.

39. Zhang, M.; Moore, R. B.; Long, T. E., *Journal of Polymer Science Part A: Polymer Chemistry* **2012,** *50* (18), 3710-3718.
40. Zhang, M.; Zhang, M.; Moore, R. B.; Long, T. E., *Polymer* **2013,** *54* (14), 3521-3528.
41. Dennis, J. M.; Fahs, G. B.; Moore, R. B.; Turner, S. R.; Long, T. E., *Macromolecules* **2014,** *47* (23), 8171-8177.
42. Knott, B. C.; Erickson, E.; Allen, M. D.; Gado, J. E.; Graham, R.; Kearns, F. L.; Pardo, I.; Topuzlu, E.; Anderson, J. J.; Austin, H. P., *Proceedings of the National Academy of Sciences* **2020,** *117* (41), 25476-25485.
43. Han, M., Depolymerization of PET bottle via methanolysis and hydrolysis. In *Recycling of Polyethylene Terephthalate Bottles*, Elsevier: 2019; pp 85-108.
44. Van Bogart, J. W. C.; Lilaonitkul, A.; Cooper, S. L., Morphology and Properties of Segmented Copolymers. In *Multiphase Polymers*, AMERICAN CHEMICAL SOCIETY: 1979; Vol. 176, pp 3-30.
45. Unal, S.; Yilgor, I.; Yilgor, E.; Sheth, J. P.; Wilkes, G. L.; Long, T. E., *Macromolecules* **2004,** *37* (19), 7081-7084.
46. Buckwalter, D. J.; Dennis, J. M.; Long, T. E., *Progress in Polymer Science* **2015,** *45*, 1-22.
47. Nomura, K.; Peng, X.; Kim, H.; Jin, K.; Kim, H. J.; Bratton, A. F.; Bond, C. R.; Broman, A. E.; Miller, K. M.; Ellison, C. J., *ACS Applied Materials & Interfaces* **2020,** *12* (8), 9726-9735.
48. Pepels, M. P. F.; Hansen, M. R.; Goossens, H.; Duchateau, R., *Macromolecules* **2013,** *46* (19), 7668-7677.
49. Maeda, T.; Kamimura, S.; Ohishi, T.; Takahara, A.; Otsuka, H., *Polymer* **2014,** *55* (24), 6245-6251.
50. Ehrenstein, M.; Dellsperger, S.; Kocher, C.; Stutzmann, N.; Weder, C.; Smith, P., *Polymer* **2000,** *41* (10), 3531-3539.
51. Vilela, C.; Silvestre, A. J. D.; Meier, M. A. R., *Macromolecular Chemistry and Physics* **2012,** *213* (21), 2220-2227.
52. Woodard, L. N.; Grunlan, M. A., *ACS macro letters* **2018,** *7* (8), 976-982.
53. Hahn, S. F., *Journal of Polymer Science Part A: Polymer Chemistry* **1992,** *30* (3), 397-408.
54. Nelson, A. M.; Pekkanen, A. M.; Forsythe, N. L.; Herlihy, J. H.; Zhang, M.; Long, T. E., *Biomacromolecules* **2017,** *18* (1), 68-76.
55. Lehman, S. E.; Wagener, K. B.; Baugh, L. S.; Rucker, S. P.; Schulz, D. N.; Varma-Nair, M.; Berluche, E., *Macromolecules* **2007,** *40* (8), 2643-2656.
56. Berg, D.; Schaefer, K.; Koerner, A.; Kaufmann, R.; Tillmann, W.; Möller, M., *Macromolecular Materials and Engineering* **2016,** *301*, 1454-1467.
57. Pelto, J.; Verho, T.; Ronkainen, H.; Kaunisto, K.; Metsäjoki, J.; Seitsonen, J.; Karttunen, M., *Polymer Testing* **2019,** *77*, 105897.
58. Mohagheghian, I.; McShane, G.; Stronge, W., *International Journal of impact engineering* **2015,** *80*, 162-176.
59. Ritter, A.; Michel, E.; Schmid, M.; Affolter, S., *Polymer Testing* **2005,** *24* (4), 498-506.
60. Ojeda, T.; Freitas, A.; Birck, K.; Dalmolin, E.; Jacques, R.; Bento, F.; Camargo, F., *Polymer Degradation and Stability* **2011,** *96* (4), 703-707.
61. Häußler, M.; Eck, M.; Rothauer, D.; Mecking, S., *Nature* **2021,** *590* (7846), 423-427.